

Releasing and Assessing the Toxicity of Polycyclic Aromatic Hydrocarbons from Biochar Loaded with Iron

Mingyu He, Peng Dai, Jiaying Lu, Yan Kang, Jian Zhang, Haiming Wu, Zhen Hu, and Zizhang Guo*

Cite This: *ACS Omega* 2023, 8, 48104–48112

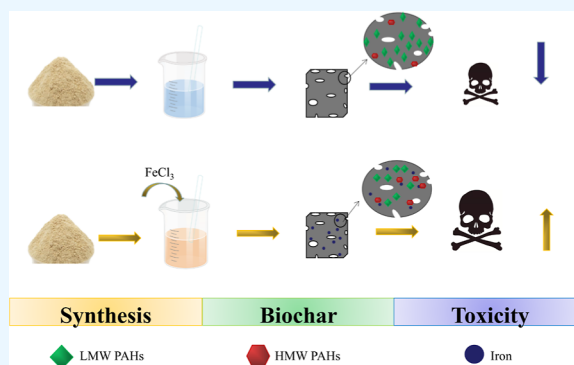
Read Online

ACCESS |

Metrics & More

Article Recommendations

ABSTRACT: Iron (Fe)-loaded biochar has garnered attention for its potential applications in recent years. However, the pyrolysis process of Fe-loaded biochar generates polycyclic aromatic hydrocarbons (PAHs), which can have adverse effects on both human health and the environment. This study explored the correlation between Fe loading and PAH production in Fe-loaded biochar. The results indicate that increasing Fe loading in biochar reduces the PAH concentration, with the most significant decrease observed in naphthalene (0.02–0.08 mg/kg). This reduction can be attributed to the decrease in precursor compounds (e.g., C_2H_2), substitution of the C=O bond by Fe–O, and a decrease in the dissolved organic matter concentration (3.19–10.76 mg/L) with Fe loading. When Fe loading increased from 0 to 10%, the ecological toxicity of biochar increased by 33.48% due to an elevated production of dibenzo[*a,h*]anthracene, which poses a significant risk to human health. Therefore, it is imperative to take into consideration the ecological risk of PAHs prior to the application of Fe-loaded biochar. This study presents a comprehensive risk assessment of Fe-loaded biochar and provides valuable insights into the optimization of its production and safe application.



1. INTRODUCTION

Biochar is a cost-effective and ecofriendly material that boasts high porosity and exceptional adsorption capacity, rendering it an ideal candidate for the removal or stabilization of contaminants in both water and soil.¹ Generally, the formation of biochar involves the depolymerization and polymerization of biomass macromolecules through intramolecular and intermolecular rearrangement reactions.^{2,3} As a result, the occurrence of polycyclic aromatic hydrocarbons (PAHs) during biochar formation is inevitable,⁴ which was a typical trace organic pollutants. In 1980, the United States Environmental Protection Agency (USEPA) has designated 16 PAHs as priority pollutants because of their significant genotoxic, mutagenic, and carcinogenic properties.^{5,6} Therefore, the production of PAHs during biochar formation has garnered increasing attention recently.

Magnetic biochar is a kind of biochar that introduces transition metals such as iron (Fe) or their oxides into its structure.^{7,8} Recently, magnetic biochar has been widely applied in wastewater treatment due to the low cost and harmlessness of Fe salts.⁹ Previous studies synthesized magnetic biochar successfully using biochar and Fe_3O_4 nanoparticles, and its removal rate of polystyrene nanoplastics reached 82.73%, which was 5.76 times that of phase original biochar.¹⁰ Zhou et al. (2020) found that when MBC activates peroxydisulfate to degrade 4-chlorophenol, the TOC removal efficiency can reach 63.5%.¹¹ Recently, Fe has been proven to

react with PAHs and eliminate them in aqueous solutions.^{12,13} However, limited information is available regarding the production of PAHs in Fe-loaded biochar, and there is still a lack of understanding about the relationship between the Fe loading amount and PAH production concentration in biochar. Furthermore, few studies have focused on the ecological risk posed by PAHs in Fe-loaded biochar,¹⁴ and the dynamic changes in ecological risk associated with Fe loading remain unclear. Therefore, it is crucial to investigate the dynamic changes in PAH production and the toxicological effects of Fe-loaded biochar.

Notably, biochar could release dissolved organic matter (DOM) during the process of wastewater treatment,^{15,16} which constitutes the majority of the dissolved fraction of biochar.¹⁷ Although DOM represents a small portion of the overall biochar, it is the most active component involved in proton and complexation reactions, and its composition and properties are essential factors influencing biochar performance.^{18,19} Previous study demonstrated that higher DOM levels can

Received: September 12, 2023

Revised: November 18, 2023

Accepted: November 21, 2023

Published: December 6, 2023



interact with the PAHs to promote and facilitate microbial degradation of PAHs.²⁰ Besides, the composition of DOM also has an influence on the elimination of PAHs. It is reported that tryptophan-like substances in DOM strengthened the electron donating capacity of DOM, which was beneficial for PAH elimination.⁶ Unfortunately, there is a paucity of studies investigating the concentration and composition of DOM released in biochar with Fe loading.

In view of the above limitations in the research field, the aims of this investigation are (1) to explore the influence of Fe loading on the concentration of 16 PAHs in biochar loaded with Fe; (2) to assess the environmental risk posed by PAHs in biochar through evaluation of their toxic equivalent quantity (TEQ); and (3) to investigate the variations in DOM and Cfree PAHs in Fe-loaded biochar as a function of Fe loading. By achieving these objectives, this study aims to contribute to a better understanding of the risks and benefits associated with Fe-loaded biochar. This will provide valuable insights for optimizing their production and safe application. Additionally, this research may help identify potential mitigation strategies for PAHs in biochar and facilitate the development of more effective methods for utilizing Fe-loaded biochar in environmental remediation and pollution control efforts.

2. MATERIALS AND METHODS

2.1. Chemical. PAH standards (a mixture of 16 PAHs, purity >97.0%) and 2-Fluorobiphenyl (C₁₂H₉F, purity >97.0%) were obtained from ANPEL Laboratory Technologies (Shanghai, China). Acetone (C₃H₆O, purity >99.5%), hexane (C₆H₁₄, purity >97%), dichloromethane (CH₂Cl₂, purity >99.5%), and methanol (CH₃OH, purity >99.8%) were all purchased from Chemical Reagent Co. Ltd. Sinopharm (Shanghai, China). All chemicals were of reagent grade or higher. Except for special instructions, the deionized water was used as an aqueous solution in this paper.

2.2. Synthesis of Fe-Loaded Biochar. Wheat straw, sourced from Dezhou, Shandong Province, was chosen as the precursor for biochar. It was ground into a fine powder using a grinder and sieved to achieve particle sizes of 400–800 μm, ensuring greater stability. FeCl₃ was impregnated into wheat straw at varying ratios of 0.1, 0.05, and 0.02 by adding 2, 1, and 0.4 g of FeCl₃ to a mixture of 20 g wheat straw and 200 mL distilled water, respectively. Blank controls were also established by adding only the same amount of wheat straw to distilled water. The impregnated precursor was vigorously agitated for 2 h using a magnetic stirrer and subsequently allowed to settle for 30 min. The supernatant was decanted, and the residual sediment was dried at 60 °C for 12 h in a constant temperature oven. The wheat straw was subjected to complete drying and subsequently heated to 600 °C at a rate of 5 °C/min using a tube furnace (STF1200) under pure nitrogen for 4 h, resulting in the production of four distinct groups of biochar with varying Fe loadings (0, 0.02, 0.05, and 0.1), designated as BC, BC-Fe0.02, BC-Fe0.05, and BC-Fe0.1.

2.3. Characterization of Biochar. The surface functional groups and microscopic morphology of the biochar were analyzed using a Fourier transform infrared spectrometer (FTIR) (Thermo Scientific Nicolet iS20) and scanning electron microscopy (SEM) (TESCAN MIRA LMS, Czech Republic), respectively. Additionally, X-ray powder diffraction (XRD) patterns of all biochar samples were performed using a Rigaku Ultima IV operated at 40 kV and 40 mA. The data were collected with a scan rate of 5° min⁻¹ within the range of

scattering angle 2θ of 10–80°. X-ray photoelectron spectroscopy (XPS) measurement was performed using a Thermo ESCALAB XI+ with Al Kα radiation to determine the element composition in biochar samples, and the binding energy was calibrated based on the C 1s peaks at 284.8 eV. A Quantachrome AUTOSORB IQ was used to measure the surface areas and pore size distribution of the sample based on the N₂ adsorption–desorption method.

2.4. PAHs Measurement. **2.4.1. Extraction of PAHs in Biochar.** PAHs were extracted from biochar using a fully automated rapid solvent extractor (Flex-HPSE). In this process, 1 g of biochar was combined with a dispersant and placed in the extraction column. Prior to extraction, 10 μL of a 100 ppm substitute (2-fluorobiphenyl) was introduced to the column to enable the calculation of PAH recovery rates. The extraction solvent was a 1:1 mixture of acetone and hexane. The operating parameters included a system pressure of 10.34 MPa, an extraction temperature of 100 °C, a heating equilibrium time of 2 min, a static extraction time of 5 min, a rinse volume of 60%, and an N₂ purge time of 60 s. The extraction cycle was repeated twice. Subsequently, the extracts were collected in a 50 mL concentration cup and reduced to 1 mL using a nitrogen-blowing apparatus.

2.4.2. Extraction of PAHs in Water. Prior to the extraction process, the C18 membrane was activated by sequential treatment with dichloromethane, methanol, and distilled water. Subsequently, a 100 pm substitute (2-fluorobiphenyl) of 50 μL was introduced into a 100 mL PAH-containing solution and transferred to the extraction column. The aqueous sample was passed through the activated C18 membrane at a flow rate of 5 mL/min. After complete processing and drying of the extraction column, 2.5 mL of dichloromethane was added to saturate the C18 membrane, followed by an additional 2.5 mL of dichloromethane for rinsing after a 5 min interval.

2.4.3. GC/MS Procedure. The determination of 16 designated priority PAHs [naphthalene (NAP), acenaphthylene (ANY), acenaphthene (ANA), fluorene (FLU), phenanthrene (PHE), anthracene (ANT), fluoranthene (FA), pyrene (PYR), benzo[*a*]anthracene (BaA), chrysene (CHR), benzo[*b*]fluoranthene (BbF), benzo[*k*]fluoranthene (BkF), benzo[*a*]pyrene (BaP), indeno[1,2,3-*cd*]perylene (IndP), dibenz[*a,h*]anthracene (DBA), and benzo[*g,h,i*]pyrene (BghiP)] by the USEPA was conducted using gas chromatography–mass spectrometry (GC–MS) following the internal standard method in accordance with the national standard HJ805-2016. The GC–MS analytical conditions included: (1) chromatographic conditions: HP-5MS capillary column (30 m × 0.25 mm × 0.25 μm); injection port temperature: 280 °C; injection volume: 1 μL; column temperature program: initial temperature of 50 °C held for 3 min, followed by a temperature ramp at a rate of 10 °C/min up to 280 °C, and maintained for 12 min (2) MS conditions: electron impact ionization (EI) source; quadrupole temperature: 150 °C; ion source temperature: 230 °C; auxiliary heating temperature: 290 °C; scan range: 45–450 *m/z*; solvent delay time: 10 min. Prior to measurement, 10 μL of phenanthrene-D10 was added to 1 mL of the extract as an internal standard.

2.4.4. Quality Ensure and Quality Control. The recovery of a substitute was 63.6–116.9% and the overall PAHs recovery rates ranged from 80.2 to 91.7%, which indicated the satisfactory performance of the extraction method. Meanwhile, limits of quantification (LOQ) were calculated using 10 times the signal-to-noise ratio (S/N). The LOQs of PAHs ranged

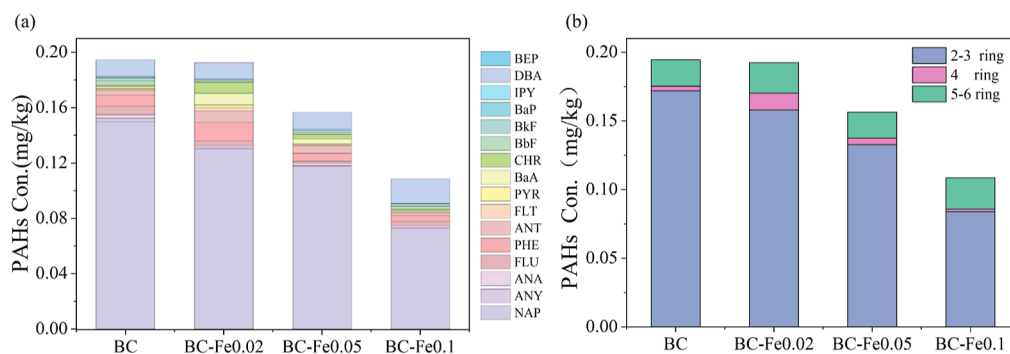


Figure 1. Concentrations of PAHs (a) and the variation in the concentrations of different rings of PAHs (b) were measured in BC, BC-Fe0.02, BC-Fe0.05, and BC-Fe0.1.

from 6.54 to 12.45 ng/L in water and 5.23–13.17 ng/kg in biochar. The concentrations of PAHs and SPAHs measured in all samples were higher than LOQ. Based on the above-mentioned parameters, the detection method achieved excellent recovery for PAHs and could ensure the accuracy of the experimental data.

2.5. Toxicity Assays. **2.5.1. Luminescence Bacteria Toxicity.** The toxicity of biochar was determined by *V. Fischeri* NRRL B-1177.²¹ Biochar samples were dissolved in 10 mL of ultrapure water and then shaken in the shaker for 6 h at 100 rpm. Afterward, the supernatant was passed through a 0.45 μm membrane, which was added to 96-well plates at 180 μL . The bacterial suspension (20 μL) was finally added, and bioluminescence inhibition was measured through multiscan spectrum (TECAN, SPARK, Switzerland) after exposure for 15 min. The control was set as a mixture of 3% sodium chloride solution and bacterial solution. The luminescence inhibition (I) of the water samples was calculated based on eq 1.

$$I = \frac{R_0 - R}{R_0} \quad (1)$$

where R and R_0 represent the relative intensity of the luminescence in samples and negative control, respectively.

2.5.2. TEQ of PAHs in Biochar. To assess the environmental risk posed by PAHs in biochar, toxic equivalent factors (TEFs) were utilized. Generally, PAHs with higher ring numbers and molecular weights exhibit greater toxicity. The TEF was established for the toxicity of PAHs by calculating their TEQ (expressed in $\mu\text{g}/\text{kg}$) using BaP as a reference for toxicity.²² Based on the TEF values, the combined toxicity of various PAHs can be expressed as a single toxic equivalent, TEQ, using the eq 2

$$\text{TEQ} = \sum (\text{TEF}_i \times C_i) \quad (2)$$

where C_i is the concentration of individual PAHs ($\mu\text{g}/\text{kg}$) and TEF is the toxicity equivalence factor.

2.6. DOM Concentration and Composition. To determine the DOM concentration in biochar, biochar samples (1.0 g) were placed in 100 mL of ultrapure water solution and then shaken in a shaker. The supernatant of the solution was collected in 1, 5, 15, 30, 60, 120, 240, and 1440 min. The biochar was filtered using a 0.22 μm filter membrane, and the water samples were analyzed for DOM concentration using a total organic carbon analyzer (Japan, Shimadzu, TOC-L).

To perform a qualitative analysis of the soluble organic matter present in biochar samples, we employed excitation–

emission matrix (EEM) spectroscopy. To facilitate the solubilization of the organic matter in biochar, each 0.5 g sample was mixed with 50 mL of deionized water and subjected to sonication using a Watson (USA) sonication bath at a power output of 30 W for 1 h. After allowing each mixture to settle for 30 min, the resulting supernatant was filtered through a 0.22 μm membrane filter (Millipore, USA). EEM spectra were obtained for each organic solution derived from the biochar samples by scanning emission spectra from 250 to 600 at 2 nm intervals and excitation wavelength ranging from 200 to 500 nm in increments of 5 nm using a fluorescence spectrophotometer.

To standardize the fluorescence signal, a reference signal was generated using ultrapure water and compared with the sample signal at the Rayleigh scattering region, following Chen et al.²³ The obtained EEM data were processed using the DOMFluor (version 1.7) toolbox in MATLAB 7.6 (MathWorks, Natick, MA, USA) for parallel factor analysis (PARAFAC) modeling. The two-to-seven-component model in PARAFAC was employed to analyze the EEMs of the samples. Nonnegative constraints were imposed on Ex and Em loadings, while residual analysis and split-half analysis were used as indicators for identifying the optimal number of individual PARAFAC components.²⁴ The maximum fluorescence intensities (F_{max}) were used to evaluate the relative concentration of each PARAFAC component.²⁵

3. RESULTS AND DISCUSSION

3.1. PAH Concentration. As depicted in Figure 1a, the variation in Fe loading within the biochar did not influence the presence of PAH types but did affect both individual PAH and total PAH concentration. The total PAH concentrations decreased significantly as the Fe loading in the biochar increased, and the total PAH concentrations of BC, BC-Fe0.02, BC-Fe0.05, and BC-Fe0.1 were 0.192, 0.186, 0.114, and 0.092 mg/kg, respectively. Compared to BC, the PAH concentration in BC-Fe0.02, BC-Fe0.05, and BC-Fe0.1 reduced by 1, 19.5, and 44.2%, respectively. NAP was found to be the most abundant PAHs in all biochar samples (ranging from 0.073 to 0.150 mg/kg), contributing to 66.8–77.0% of total PAHs. PHE was the second most abundant PAH (0.004–0.013 mg/kg) in all biochar samples, followed by FLU (0.001–0.006 mg/kg). Generally, 2–3 ring PAHs were considered as the low-molecular-weight (LMW) PAH, and 5–6 PAHs were considered as the high-molecular-weight (HMW) PAH.²⁶ Figure 1b summarizes the variation in release concentration of different rings of PAHs, revealing a significant gradual decrease

($p < 0.05$) in LMW PAHs with increasing Fe loading. Particularly, the concentration of NAP decreased most (0.019–0.077 mg/kg) with the increasing Fe loading. Additionally, there were no significant changes in HMW PAH concentration. However, it is noted that the concentration of DBA increased with the increase of Fe loading, and the DBA concentration of BC-Fe0.1 was highest (0.018 mg/kg). DBA is a kind of 5-ring PAH which had a higher toxicity risk to human health compared with LMW PAHs.²⁷ Therefore, this result implied that the toxicity of biochar might increase with the increase of Fe loading (detail in Section 3.3).

3.2. Characterization of Biochar. The physicochemical properties of all biochar samples were characterized to illustrate the mechanism of PAH generation in biochar. The SEM images presented in Figure 2 clearly demonstrate the

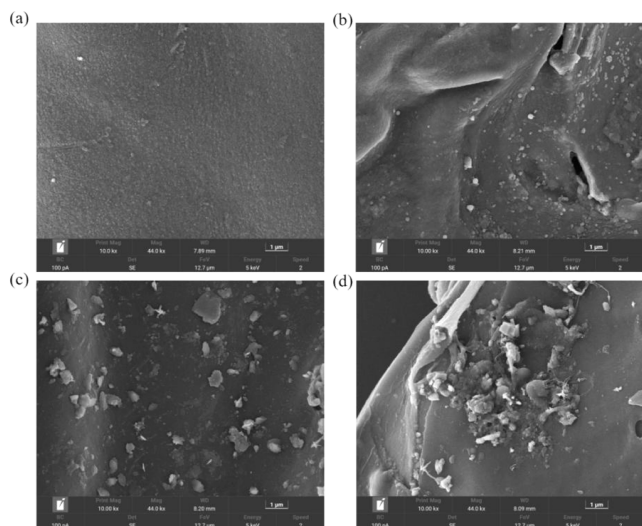


Figure 2. SEM images of (a) BC, (b) BC-Fe0.02, (c) BC-Fe0.05, and (d) BC-Fe0.1.

morphological differences between BC and Fe-loaded biochar. The surface of BC appears smooth and dense, whereas spherical and striated particles with a coarse and porous texture are visible on the surfaces of BC-Fe0.02, BC-Fe0.05, and BC-Fe0.1. These observations suggest that Fe was successfully loaded onto the biochar. Notably, the roughness of biochar increased with the increase of iron load (Figure 2), which increased the iron exposure and reaction to PAHs, potentially leading to a reduction in PAH release.

The XRD diffraction pattern of biochar with different Fe loading is shown in Figure 3a, which showed that a typical diffraction peak of C (26.603° JCPDS PDF# 26-1076) was observed in all biochar samples. The intensity of C was decreased with the increase of Fe loading. Additionally, a typical diffraction peak of Fe₂O₃ (40.854° JCPDS PDF# 33-0664) was observed in BC-Fe0.02, BC-Fe0.05, and BC-Fe0.1, and another typical diffraction peak of Fe₂O₃ (54.935° JCPDS PDF# 47-1409) was only shown in BC-Fe0.1. XPS was utilized to analyze the surface element and composition, chemical state of biochar prepared in this study.²⁸ The XPS spectrogram (Figure 3b) showed that a peak at 710 eV, attributing to Fe element,¹³ was present in BC-Fe0.02, BC-Fe0.05, and BC-Fe0.1, while it was absent in BC alone. This result indicated that the Fe loading into the aforementioned biochar samples was successful.

FTIR spectroscopy was employed to identify the functional groups that are present on the surface of biochar. The FTIR spectrum of BC exhibits 9 distinct absorption peaks (Figure 3c), which are characteristic of organic structures typically associated with wheat straw feedstock. Wheat straw is composed of approximately 30% cellulose, 50% hemicellulose, and 15% lignin.²⁹ The FTIR spectra of hemicellulose, cellulose, and lignin have been reported in previous studies,³⁰ and these three components primarily consist of alkene hydrocarbon esters, aromatic compounds, ketones, and alcohols with various oxygen-containing functional groups. For example, the O–H (3400–3200 cm⁻¹), C=O (1567 cm⁻¹), and C–O–H (~1050 cm⁻¹) bands, as well as the aliphatic C–O–C and C–OH bands (1160–1030 cm⁻¹), represent the oxidation functional groups of cellulose.^{31,32} In contrast, the FTIR spectrum of BC-Fe0.02, BC-Fe0.05, and BC-Fe0.1 is relatively simple with only three distinct absorption peaks corresponding to –OH at 3450 cm⁻¹, C=C in water molecules at 1637 cm⁻¹, and C–H/C–O/Fe–O at 460 cm⁻¹ structures, respectively. Previous studies have also supported the combination of metal oxides with chemical functional groups (such as C=O) on hybrids.^{12,33} This comparison demonstrates that the modification of biochar results in a larger number of –OH functional groups. Moreover, the broad peak at 460 cm⁻¹ in the sample contains a characteristic peak related to the bending vibration of the Fe–O bond, which is typical of low-crystallinity water ferrite.³⁴ The absence of an absorption peak in the organic structure of biochar is likely due to the tight encapsulation of the Fe–O groups. Both XPS and FTIR results demonstrated that iron was loaded and encapsulated in biochar. Furthermore, the disappearance of C=O bonds and

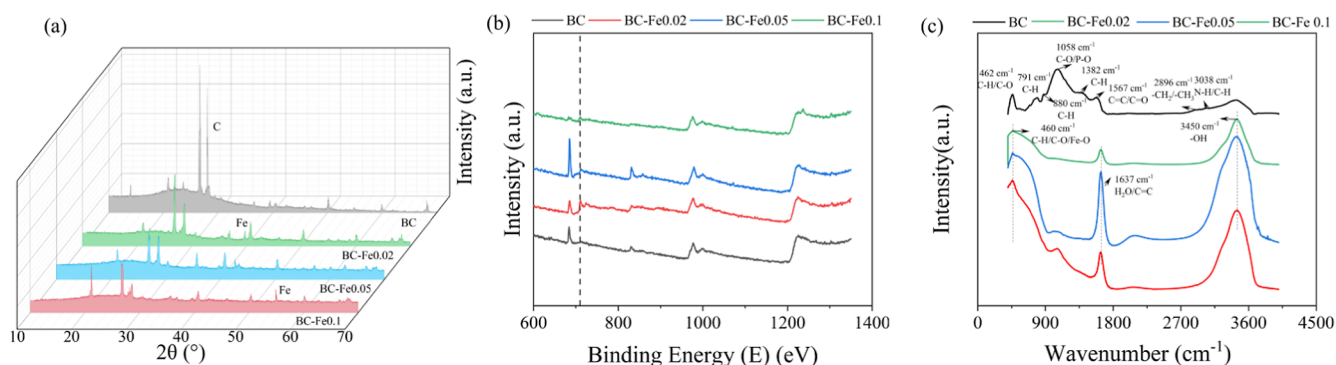


Figure 3. XRD (a), XPS (b), and FTIR (c) spectrograms of BC, BC-Fe0.02, BC-Fe0.05, and BC-Fe0.1.

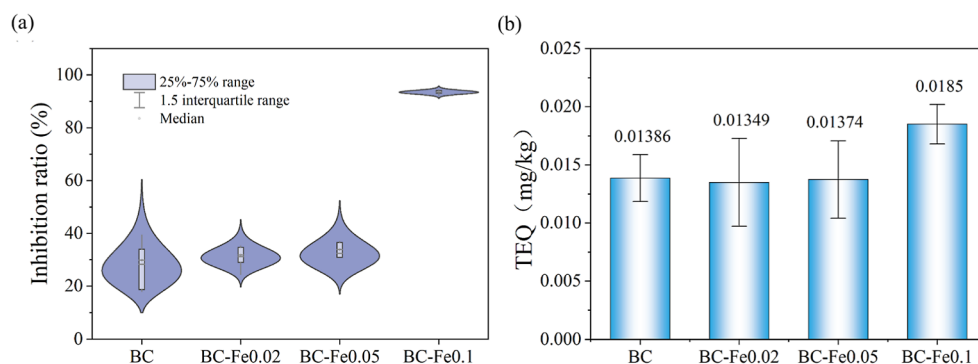


Figure 4. (a) Luminescence bacteria toxicity and (b) TEQ of biochar with different Fe loadings.

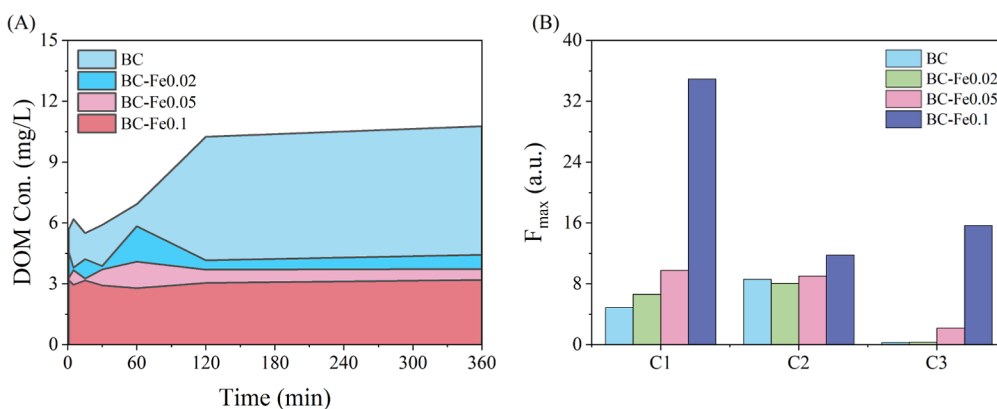


Figure 5. (A) DOM concentration and (B) their corresponding fluorescence intensities by EEM-PARAFAC analysis in the DOM of biochar with different Fe loadings.

the appearance and increase of Fe–O and –OH groups were observed in BC-Fe0.02, BC-Fe0.05, and BC-Fe0.1. The substitution of the C=O bond by Fe–O, indicated by the change in functional groups upon iron addition, may lead to a reduced release of PAHs due to Fe-mediated oxidation. Therefore, an increase in Fe loading resulted in a decrease in the concentration of released PAHs.

3.3. Identification of Biochar Toxicity. The concentrations of PAHs in the biochar samples, including BC, BC-Fe0.02, BC-Fe0.05, and BC-Fe0.1 were determined to be 0.192, 0.186, 0.113797, and 0.0921 mg/kg, respectively. The international biochar initiative has established a threshold range of PAHs in biochar from 6 to 20 mg/kg. The European biochar certificate also establishes limits for the concentration of PAHs in basic and premium biochar with the latter having a more stringent limit of less than 4 mg/kg. These results indicate that all biochar samples meet the criteria for high-quality biochar. Previous studies have also observed the formation of PAHs during pyrolysis, regardless of biomass type, but at concentrations deemed acceptable under Germany's Federal Soil Protection (Basic quality scenario).^{35,36}

However, it should be noted that relying solely on the total concentration of these 16 PAHs may not provide a comprehensive assessment of the environmental risk associated with biochar, potentially leading to significant underestimation of the actual risk posed by organic pollutants.³⁷ Therefore, luminescence bacteria toxicity was utilized as a measure to evaluate the environmental risk of PAHs more accurately.³⁸ It could be seen from Figure 4a that the average inhibition of BC, BC-Fe0.02, BC-Fe0.05, and BC-Fe0.1 was 28.29, 31.28, 32.38,

and 93.45%, respectively. This result indicated that the ecological toxicity of biochar was enhanced with the increase of Fe loading. Additionally, TEQ was an important parameter that could evaluate environmental risk.²⁶ As depicted in Figure 4b, the TEQ values for BC, BC-Fe0.02, BC-Fe0.05, and BC-Fe0.1 were calculated to be 0.014, 0.013, 0.014, and 0.018 mg/kg, respectively. The results indicated an increasing trend of TEQ values with higher Fe loading, which was in line with the result of luminescence bacteria toxicity. The environmental ecological risk is influenced not only by the concentration of PAHs but also by the kind of PAHs and their chemical structures. Despite a gradual decrease in PAH concentrations with the increase of Fe loading, the concentration of DBA, which is a typical HMW PAH and possesses extremely high toxicity, was enhanced with increasing Fe loading. As reported previously, the toxicity of DBA is hundreds or thousands of times more toxic than LMW PAHs.^{26,39} As a result, although the concentration of PAHs decreased, the ecological toxicity of BC-Fe0.1 was highest due to the higher concentration of DBA. Therefore, more attention should be paid to the ecological risk of Fe-loaded PAHs.

3.4. DOM Concentration and Composition. Biochar-derived DOM encompasses a spectrum of diverse organic molecules varying in size and structure, which can pass through a 0.45 μm filter and release into the water body.^{40,41} The dynamic DOM-released concentration of different biochar samples is shown in Figure 5a, which showed that the DOM concentration varied in the first 0–120 min and gradually stabilized after 120 min. The DOM concentration of BC, BC-Fe0.02, BC-Fe0.05, and BC-Fe0.1 was 10.76, 4.43, 3.73, and 3.19 mg/L, respectively, which showed that DOM concen-

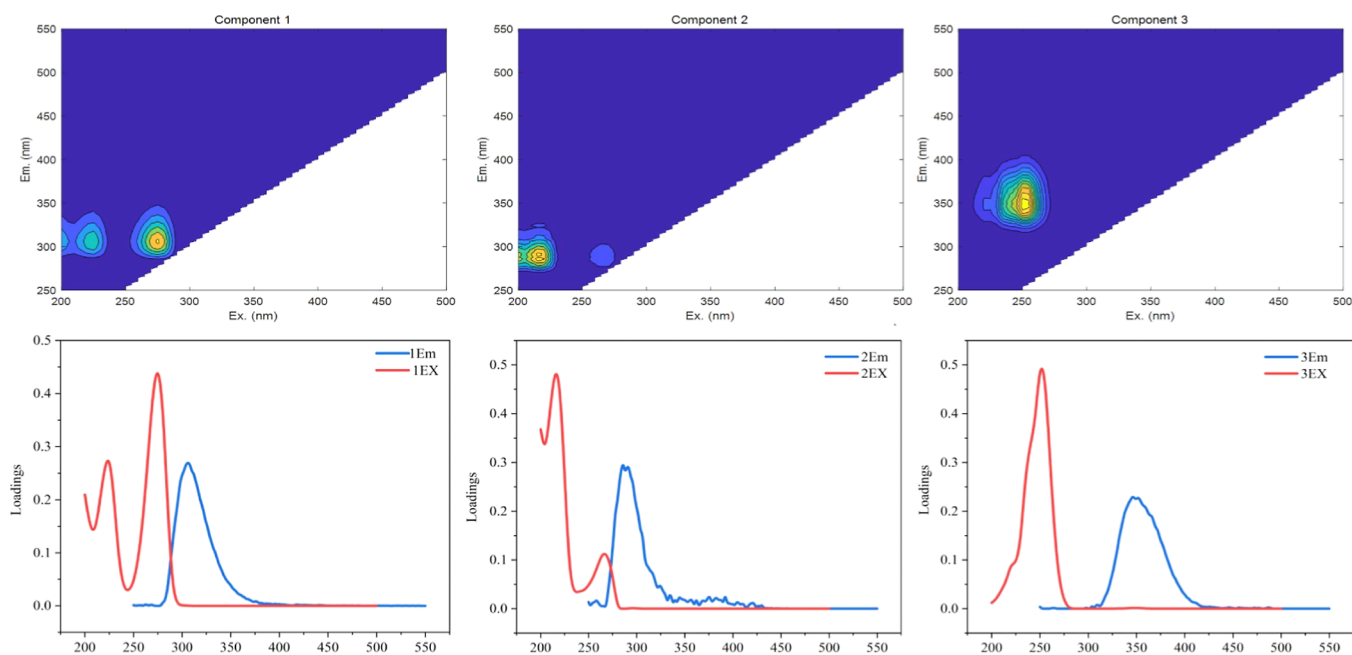


Figure 6. EEM contours and spectral loadings of the three components were identified by fluorescence-PARAFAC analysis.

tration was reduced with the increasing Fe loading. This result might be due to the reaction between Fe and DOM, which formed Fe-DOM complexes and promoted the sequestration of organic carbon.⁴² Fe-DOM complexes could promote the synthesis and transformation of organic matter,⁴³ which might promote the synthesis and production of DBA. In addition, DOM was an important carrier for PAHs, and a higher DOM concentration was beneficial for the existence of PAHs.^{44,45} Therefore, the decrease in the DOM concentration is also the reason for the decrease in PAH concentration with the increasing Fe loading.

PARAFAC was utilized to analyze the DOM composition in the biochar sample. As shown in Figure 6, three fluorescent components (C1–C3) were identified by PARAFAC. Component 1 (C1) is expected to contain substances resembling tryptophan, exhibiting two peaks at 225/322 nm (Ex/Em) and 285/322 nm (Ex/Em), respectively.⁴⁶ Component 2 (C2) exhibits two peaks at 220/300 nm (Ex/Em) and 265/300 nm (Ex/Em), resembling the spectral characteristics of tyrosine-like substance,^{46,47} while component 3 (C3) displays a maximum at 250/350 nm, indicating its similarity to tyrosine-like substance.⁴⁸ Notably, the intensity of tryptophan was significantly enhanced with the increase of Fe loading, which was also in line with previous studies.⁴⁹ Tryptophan was reported to be played an important role in the electron transfer process,⁵⁰ which could be in favor of the reaction between Fe and PAHs and decrease the PAH concentration. Besides, three DOM substances can be classified into two main groups: protein-like and soluble microbial byproduct-like substances, which have a high potential for microbial utilization and can serve as a significant source of carbon for microbial communities.⁵¹ Hence, the interspecific electron transfer could be enhanced in the microbial community and benefit for the remediation of PAHs with Fe-loaded biochar application. It has been demonstrated that Bacteroidetes, Alpha-, and Betaproteobacteria were the particularly dominant phylum in response to

elevated DOM levels, and proteobacteria were considered the dominant phylum in degrading PAHs.⁵²

3.5. Proposed Mechanism of Fe Influence on the Production of PAHs in Biochar. Three mechanisms for PAH generation during biochar pyrolysis were identified, including acetylene additions, vinylacetylene additions, and radical reactions. Among them, the hydrogen extraction acetylene addition reaction was considered as the primary mechanism.⁵³ This mechanism involves a two-step process that relies on the repetitive sequence of hydrogen abstraction to activate the aromatic molecule, followed by acetylene (C_2H_2) addition to the radical site formed during the hydrogen abstraction step.⁵⁴ Hence, C_2H_2 and the benzene ring are crucial precursors of PAH generation during biochar pyrolysis. Cellulose was the main component of wheat straw and could produce PAHs by Diels–Alder type reactions.⁵⁵ Fe plays an important role in impeding the degradation of cellulose that produces a large number of small organic compounds such as C_2H_2 during the carbonization. In addition, previous studies reported that the presence of inorganic substances can result in a 50% reduction in L-glucan yield.⁵³ L-glucan is a key intermediate that will undergo dehydration, C–O bond breaking, and C–C bond breaking to form benzene rings. In summary, Fe could reduce the important precursors (i.e., C_2H_2 and benzene ring), which inhibited the generation of PAHs, and thus PAH concentration was decreased with the increasing $FeCl_3$. Compared with HMW PAHs, LMW PAHs possessed lower stability property and higher reaction activity,²² and thus Fe could react with LMW PAHs easily to eliminate the LWH PAHs production in Fe-loaded biochar. This was the reason LMW PAHs decreased significantly with increasing Fe loading. Additionally, the decreased DOM concentration and enhanced tryptophan intensity with the increase of Fe loading also led to a decrease in the production of PAHs. Notably, the increased Fe loading in biochar resulted in an increased release of DBA into the environment that increased the ecological toxicity of PAHs. Therefore, it is necessary to take into consideration the

ecological risk assessment of PAHs prior to the application of Fe-loaded biochar.

4. CONCLUSIONS

In this study, it was found that Fe-loading reducing precursor compounds such as C₂H₂ and cyclopentadiene resulted in a reduction in PAH concentration in the biochar. The substitution of the C=O bond by Fe–O and the concentration of DOM decreases also explain the decrease in PAH production. However, the ecological toxicity of biochar enhanced with Fe loading because of the enhanced DBA production. Therefore, it is imperative to consider the ecological risk assessment of PAHs prior to the application of iron-loaded biochar, particularly considering influential factors such as pyrolysis temperature and iron content.

■ AUTHOR INFORMATION

Corresponding Author

Zizhang Guo – Key Laboratory of Ecological Impacts of Hydraulic-projects and Restoration of Aquatic Ecosystem of Ministry of Water Resources, Wuhan 430079, China; Shandong Key Laboratory of Water Pollution Control and Resource Reuse, School of Environmental Science and Engineering, Shandong University, Qingdao 266237, China; orcid.org/0000-0002-0099-8013; Email: guozizhang@sdu.edu.cn

Authors

Mingyu He – Key Laboratory of Ecological Impacts of Hydraulic-projects and Restoration of Aquatic Ecosystem of Ministry of Water Resources, Wuhan 430079, China; Shandong Key Laboratory of Water Pollution Control and Resource Reuse, School of Environmental Science and Engineering, Shandong University, Qingdao 266237, China

Peng Dai – Department of Civil & Environmental Engineering, South Dakota State University, Brookings, South Dakota 57007, United States; orcid.org/0000-0002-5901-1500

Jiaxing Lu – Shandong Key Laboratory of Water Pollution Control and Resource Reuse, School of Environmental Science and Engineering, Shandong University, Qingdao 266237, China

Yan Kang – College of Environment and Safety Engineering, Qingdao University of Science and Technology, Qingdao 266042, China; orcid.org/0000-0002-3773-9170

Jian Zhang – Shandong Key Laboratory of Water Pollution Control and Resource Reuse, School of Environmental Science and Engineering, Shandong University, Qingdao 266237, China; orcid.org/0000-0003-4952-2785

Haiming Wu – Shandong Key Laboratory of Water Pollution Control and Resource Reuse, School of Environmental Science and Engineering, Shandong University, Qingdao 266237, China

Zhen Hu – Shandong Key Laboratory of Water Pollution Control and Resource Reuse, School of Environmental Science and Engineering, Shandong University, Qingdao 266237, China; orcid.org/0000-0002-4728-945X

Complete contact information is available at:
<https://pubs.acs.org/10.1021/acsomega.3c06950>

Author Contributions

The manuscript was written through contributions of all authors. All authors have given approval to the final version of the manuscript.

Notes

The authors declare no competing financial interest.

■ ACKNOWLEDGMENTS

This work was supported by the Key Laboratory of Ecological Impacts of Hydraulic-projects and Restoration of Aquatic Ecosystem of Ministry of Water Resources (KL-MWR-202104) and the National Natural Science Foundation of China (no. 51925803, 52270158, and 51908326).

■ REFERENCES

- (1) Zhang, Z.; Zhu, Z.; Shen, B.; Liu, L. Insights into biochar and hydrochar production and applications: A review. *Energy* **2019**, *171*, 581–598.
- (2) Buss, W.; Graham, M. C.; MacKinnon, G.; Mašek, O. Strategies for producing biochars with minimum PAH contamination. *J. Anal. Appl. Pyrolysis* **2016**, *119*, 24–30.
- (3) De la Rosa, J. M.; Paneque, M.; Hilber, I.; Blum, F.; Knicker, H. E.; Bucheli, T. D. Assessment of polycyclic aromatic hydrocarbons in biochar and biochar-amended agricultural soil from Southern Spain. *J. Soils Sediments* **2016**, *16* (2), 557–565.
- (4) McGrath, T. E.; Chan, W. G.; Hajaligol, M. R. Low temperature mechanism for the formation of polycyclic aromatic hydrocarbons from the pyrolysis of cellulose. *J. Anal. Appl. Pyrolysis* **2003**, *66* (1–2), 51–70.
- (5) Dang, J.; Shi, X.; Hu, J.; Chen, J.; Zhang, Q.; Wang, W. Mechanistic and kinetic studies on OH-initiated atmospheric oxidation degradation of benzo alpha pyrene in the presence of O₂ and NO_x. *Chemosphere* **2015**, *119*, 387–393.
- (6) Lu, J.; Guo, Z.; He, M.; Hu, Z.; Wu, H.; Zhuang, L.; Kong, Q.; Zhang, J. Highly enhanced removal of nutrients and benzo[a]pyrene in a siphon constructed wetland with magnetite: Performance and mechanisms. *Chem. Eng. J.* **2022**, *446*, 136895.
- (7) Yi, Y.; Huang, Z.; Lu, B.; Xian, J.; Tsang, E. P.; Cheng, W.; Fang, J.; Fang, Z. Magnetic biochar for environmental remediation: A review. *Bioresour. Technol.* **2020**, *298* (298), 122468.
- (8) Tong, M.; He, L.; Rong, H.; Li, M.; Kim, H. Transport behaviors of plastic particles in saturated quartz sand without and with biochar/Fe₃O₄-biochar amendment. *Water Res.* **2020**, *169* (169), 115284.
- (9) Shi, S.; Yang, J.; Liang, S.; Li, M.; Gan, Q.; Xiao, K.; Hu, J. Enhanced Cr(VI) removal from acidic solutions using biochar modified by Fe₃O₄@SiO₂-NH₂ particles. *Sci. Total Environ.* **2018**, *628–629*, 499–508.
- (10) Shi, Q.; Guo, S.; Tang, J.; Lyu, H.; Ri, C.; Sun, H. Enhanced removal of aged and differently functionalized polystyrene nano-plastics using ball-milled magnetic pinewood biochars. *Environ. Pollut.* **2023**, *316*, 120696.
- (11) Zhou, H.; Zhu, X.; Chen, B. Magnetic biochar supported α-MnO₂ nanorod for adsorption enhanced degradation of 4-chlorophenol via activation of peroxydisulfate. *Sci. Total Environ.* **2020**, *724*, 138278.
- (12) Lu, J.; Guo, Z.; Li, M.; He, M.; Zhen, J.; Ni, B.-J.; Zhang, J. Manganese ore enhanced polycyclic aromatic hydrocarbons removal in constructed wetlands: Insights into the key removal mechanism and main driving factor. *Chem. Eng. J.* **2023**, *467*, 143430.
- (13) Lu, J.; Guo, Z.; Pan, Y.; Li, M.; Chen, X.; He, M.; Wu, H.; Zhang, J. Simultaneously enhanced removal of PAHs and nitrogen driven by Fe²⁺/Fe³⁺ cycle in constructed wetland through automatic tidal operation. *Water Res.* **2022**, *215*, 118232.
- (14) Harmsen, J.; Naidu, R. Bioavailability as a tool in site management. *J. Hazard. Mater.* **2013**, *261*, 840–846.

- (15) Graber, E. R.; Tsechansky, L.; Lew, B.; Cohen, E. Reducing capacity of water extracts of biochars and their solubilization of soil Mn and Fe. *Eur. J. Soil Sci.* **2014**, *65* (1), 162–172.
- (16) Feng, Z.; Fan, Z.; Song, H.; Li, K.; Lu, H.; Liu, Y.; Cheng, F. Biochar induced changes of soil dissolved organic matter: The release and adsorption of dissolved organic matter by biochar and soil. *Sci. Total Environ.* **2021**, *783*, 147091.
- (17) Li, M.; Zhang, A.; Wu, H.; Liu, H.; Lv, J. Predicting potential release of dissolved organic matter from biochars derived from agricultural residues using fluorescence and ultraviolet absorbance. *J. Hazard. Mater.* **2017**, *334*, 86–92.
- (18) Rajapaksha, A. U.; Ok, Y. S.; El-Naggar, A.; Kim, H.; Song, F.; Kang, S.; Tsang, Y. F. Dissolved organic matter characterization of biochars produced from different feedstock materials. *J. Environ. Manage.* **2019**, *233*, 393–399.
- (19) Smith, C. R.; Hatcher, P. G.; Kumar, S.; Lee, J. W. Investigation into the Sources of Biochar Water-Soluble Organic Compounds and Their Potential Toxicity on Aquatic Microorganisms. *ACS Sustain. Chem. Eng.* **2016**, *4* (5), 2550–2558.
- (20) Kang, Y.; Ma, H.; Jing, Z.; Zhu, C.; Li, Y.; Wu, H.; Dai, P.; Guo, Z.; Zhang, J. Enhanced benzofluoranthrene removal in constructed wetlands with iron-modified biochar: Mediated by dissolved organic matter and microbial response. *J. Hazard. Mater.* **2023**, *443*, 130322.
- (21) Sredlova, K.; Skrob, Z.; Filipova, A.; Mašín, P.; Holecova, J.; Cajthaml, T. Biodegradation of PCBs in contaminated water using spent oyster mushroom substrate and a trickle-bed bioreactor. *Water Res.* **2020**, *170*, 115274.
- (22) Lu, J.; Zhang, J.; Xie, H.; Wu, H.; Jing, Y.; Ji, M.; Hu, Z. Transformation and toxicity dynamics of polycyclic aromatic hydrocarbons in a novel biological-constructed wetland-microbial wastewater treatment process. *Water Res.* **2022**, *223*, 119023.
- (23) Chen, W.; Westerhoff, P.; Leenheer, J. A.; Booksh, K. Fluorescence excitation-emission matrix regional integration to quantify spectra for dissolved organic matter. *Environ. Sci. Technol.* **2003**, *37* (24), 5701–5710.
- (24) He, W.; Lee, J.-H.; Hur, J. Anthropogenic signature of sediment organic matter probed by UV-Visible and fluorescence spectroscopy and the association with heavy metal enrichment. *Chemosphere* **2016**, *150*, 184–193.
- (25) Zhou, X.; Chen, Z.; Li, Z.; Wu, H. Impacts of aeration and biochar addition on extracellular polymeric substances and microbial communities in constructed wetlands for low C/N wastewater treatment: Implications for clogging. *Chem. Eng. J.* **2020**, *396*, 125349.
- (26) Saber, A. N.; Zhang, H.; Islam, A.; Yang, M. Occurrence, fates, and carcinogenic risks of substituted polycyclic aromatic hydrocarbons in two coking wastewater treatment systems. *Sci. Total Environ.* **2021**, *789*, 147808.
- (27) Ndifet, C. M. T.; Ze Bilo'o, P.; Anombogo, G. A. M.; Kom Regonne, R.; Ngassoum, M. B. The study of three beaches of South-West Cameroon polluted by polycyclic aromatic hydrocarbons. *Environ. Monit. Assess.* **2023**, *195* (4), 506.
- (28) Mo, S.; Zhang, Q.; Li, J.; Sun, Y.; Ren, Q.; Zou, S.; Zhang, Q.; Lu, J.; Fu, M.; Mo, D.; Wu, J.; Huang, H.; Ye, D. Highly efficient mesoporous MnO₂ catalysts for the total toluene oxidation: Oxygen-Vacancy defect engineering and involved intermediates using in situ DRIFTS. *Appl. Catal., B* **2020**, *264*, 118464.
- (29) Kumari, D.; Singh, R. Pretreatment of lignocellulosic wastes for biofuel production: A critical review. *Renewable Sustainable Energy Rev.* **2018**, *90*, 877–891.
- (30) Calderon, F. J.; McCarty, G. W.; Reeves, J. B. Pyrolysis-MS and FT-IR analysis of fresh and decomposed dairy manure. *J. Anal. Appl. Pyrolysis* **2006**, *76* (1–2), 14–23.
- (31) Shen, H.; Huang, Y.; Wang, R.; Zhu, D.; Li, W.; Shen, G.; Wang, B.; Zhang, Y.; Chen, Y.; Lu, Y.; Chen, H.; Li, T.; Sun, K.; Li, B.; Liu, W.; Liu, J.; Tao, S. Global Atmospheric Emissions of Polycyclic Aromatic Hydrocarbons from 1960 to 2008 and Future Predictions. *Environ. Sci. Technol.* **2013**, *47* (12), 6415–6424.
- (32) Bustin, R. M.; Guo, Y. Abrupt changes (jumps) in reflectance values and chemical compositions of artificial charcoals and inertinite in coals. *Int. J. Coal Geol.* **1999**, *38* (3–4), 237–260.
- (33) Zhang, Y.; Nan, Z. Preparation of magnetic ZnLa_{0.02}-Fe_{1.98}O₄/MWCNTs composites and investigation on its adsorption of methyl orange from aqueous solution. *Mater. Res. Bull.* **2015**, *66*, 176–185.
- (34) Salunkhe, M. Y.; Choudhary, D. S.; Kulkarni, D. K. Infrared absorption studies of the system Sr₂Me₂Fe₁₂O₂₂. *Vib. Spectrosc.* **2004**, *34* (2), 221–224.
- (35) Kończak, M.; Gao, Y.; Oleszczuk, P. Carbon dioxide as a carrier gas and biomass addition decrease the total and bioavailable polycyclic aromatic hydrocarbons in biochar produced from sewage sludge. *Chemosphere* **2019**, *228*, 26–34.
- (36) Yang, X.; Ng, W.; Wong, B. S. E.; Baeg, G. H.; Wang, C.-H.; Ok, Y. S. Characterization and ecotoxicological investigation of biochar produced via slow pyrolysis: Effect of feedstock composition and pyrolysis conditions. *J. Hazard. Mater.* **2019**, *365*, 178–185.
- (37) Hale, S. E.; Lehmann, J.; Rutherford, D.; Zimmerman, A. R.; Bachmann, R. T.; Shitumbanuma, V.; O'Toole, A.; Sundqvist, K. L.; Arp, H. P. H.; Cornelissen, G. Quantifying the Total and Bioavailable Polycyclic Aromatic Hydrocarbons and Dioxins in Biochars. *Environ. Sci. Technol.* **2012**, *46* (5), 2830–2838.
- (38) Tang, L.; Ma, X. Y.; Wang, Y.; Zhang, S.; Zheng, K.; Wang, X. C.; Lin, Y. Removal of trace organic pollutants (pharmaceuticals and pesticides) and reduction of biological effects from secondary effluent by typical granular activated carbon. *Sci. Total Environ.* **2020**, *749*, 141611.
- (39) Aziz, F.; Syed, J. H.; Malik, R. N.; Katsoyiannis, A.; Mahmood, A.; Li, J.; Zhang, G.; Jones, K. C. Occurrence of polycyclic aromatic hydrocarbons in the Soan River, Pakistan: Insights into distribution, composition, sources and ecological risk assessment. *Ecotoxicol. Environ. Saf.* **2014**, *109*, 77–84.
- (40) Kuo, Y.-L.; Lee, C.-H.; Jien, S.-H. Reduction of Nutrient Leaching Potential in Coarse-Textured Soil by Using Biochar. *Water* **2020**, *12* (7), 2012.
- (41) Swaren, L.; Safari, S.; Konhauser, K. O.; Alessi, D. S. Pyrolyzed biomass-derived nanoparticles: a review of surface chemistry, contaminant mobility, and future research avenues to fill the gaps. *Biochar* **2022**, *4* (1), 33.
- (42) Sharma, P.; Ofner, J.; Kappler, A. Formation of Binary and Ternary Colloids and Dissolved Complexes of Organic Matter, Fe and As. *Environ. Sci. Technol.* **2010**, *44* (12), 4479–4485.
- (43) Che, C.-M.; Zhou, C.-Y.; Wong, E. L.-M. Catalysis by Fe = X Complexes (X = NR, CR₂). In *Iron Catalysis: Fundamentals and Applications*; Plietker, B., Ed.; Springer, 2011, pp 111–138.
- (44) Sun, Y.; Zhang, S.; Xie, Z.; Lan, J.; Li, T.; Yuan, D.; Yang, H.; Xing, B. Characteristics and ecological risk assessment of polycyclic aromatic hydrocarbons in soil seepage water in karst terrains, southwest China. *Ecotoxicol. Environ. Saf.* **2020**, *190*, 110122.
- (45) Sheng, Y.; Yan, C.; Nie, M.; Ju, M.; Ding, M.; Huang, X.; Chen, J. The partitioning behavior of PAHs between settled dust and its extracted water phase: Coefficients and effects of the fluorescent organic matter. *Ecotoxicol. Environ. Saf.* **2021**, *223*, 112573.
- (46) Chen, W.; Westerhoff, P.; Leenheer, J. A.; Booksh, K. Fluorescence Excitation–Emission Matrix Regional Integration to Quantify Spectra for Dissolved Organic Matter. *Environ. Sci. Technol.* **2003**, *37* (24), 5701–5710.
- (47) Li, W.-T.; Chen, S.-Y.; Xu, Z.-X.; Li, Y.; Shuang, C.-D.; Li, A.-M. Characterization of Dissolved Organic Matter in Municipal Wastewater Using Fluorescence PARAFAC Analysis and Chromatography Multi-Excitation/Emission Scan: A Comparative Study. *Environ. Sci. Technol.* **2014**, *48* (5), 2603–2609.
- (48) Ferretto, N.; Tedetti, M.; Guigue, C.; Mounier, S.; Redon, R.; Goutx, M. Identification and quantification of known polycyclic aromatic hydrocarbons and pesticides in complex mixtures using fluorescence excitation-emission matrices and parallel factor analysis. *Chemosphere* **2014**, *107*, 344–353.

(49) Li, M.; Li, J.; Zhao, L.; Liu, S.; Wang, Y.; Bian, H. Effects of exogenous Fe addition on soil respiration rate and dissolved organic carbon structure in temperate forest swamps of northeastern China. *Environ. Res.* **2023**, *216*, 114800.

(50) Natali, M.; Amati, A.; Demitri, N.; Iengo, E. Photoinduced Electron vs. Concerted Proton Electron Transfer Pathways in Sn-IV (l-Tryptophanato)(2) Porphyrin Conjugates. *Chem.—Eur. J.* **2021**, *27* (29), 7872–7881.

(51) Jones, D. L.; Murphy, D. V.; Khalid, M.; Ahmad, W.; Edwards-Jones, G.; DeLuca, T. H. Short-term biochar-induced increase in soil CO₂ release is both biotically and abiotically mediated. *Soil Biol. Biochem.* **2011**, *43* (8), 1723–1731.

(52) Li, Y.; Xu, C.; Zhang, W.; Lin, L.; Wang, L.; Niu, L.; Zhang, H.; Wang, P.; Wang, C. Response of bacterial community in composition and function to the various DOM at river confluences in the urban area. *Water Res.* **2020**, *169*, 115293.

(53) Reizer, E.; Viskolcz, B.; Fiser, B. Formation and growth mechanisms of polycyclic aromatic hydrocarbons: A mini-review. *Chemosphere* **2022**, *291*, 132793.

(54) Liu, W.-J.; Li, W.-W.; Jiang, H.; Yu, H.-Q. Fates of Chemical Elements in Biomass during Its Pyrolysis. *Chem. Rev.* **2017**, *117* (9), 6367–6398.

(55) Nan, H.; Yang, F.; Zhao, L.; Mašek, O.; Cao, X.; Xiao, Z. Interaction of Inherent Minerals with Carbon during Biomass Pyrolysis Weakens Biochar Carbon Sequestration Potential. *ACS Sustain. Chem. Eng.* **2019**, *7* (1), 1591–1599.